RESEARCH ARTICLE SUMMARY

CELL BIOLOGY

Mitochondria shed their outer membrane in response to infection-induced stress

Xianhe Li, Julian Straub, Tânia Catarina Medeiros, Chahat Mehra, Fabian den Brave, Esra Peker, Ilian Atanassov, Katharina Stillger, Jonas Benjamin Michaelis, Emma Burbridge, Colin Adrain, Christian Münch, Jan Riemer, Thomas Becker, Lena F. Pernas*

INTRODUCTION: Mitochondria are dynamic organelles that coordinate many cellular functions that are essential for life, including diverse metabolic processes, cell division and differentiation, and immune signaling.

To carry out these diverse functions, mitochondria must communicate with the cytosol, a task mediated by the outer mitochondrial membrane (OMM), the gateway between mitochondria and the rest of the cell. Thus, preserving the integrity of the OMM is essential for cellular homeostasis. Although responses to stress that is artificially induced by small molecules have been described, little is known of the mechanisms by which mammalian cells respond to naturally occurring stresses of the OMM.

RATIONALE: Several intracellular microbes come in contact with the host OMM or release proteins that target the OMM. We reasoned that microbial infection would serve as a model with which to study cellular responses to natural OMM stress. To this end, we chose the human parasite *Toxoplasma gondii* because it tethers host mitochondria to its parasite vacuole; in an infected cell, areas of close membrane apposition form between the host OMM and the parasite vacuole membrane. To address how *Toxoplasma* affected the OMM, we performed live-cell imaging of infected mammalian cells stably expressing OMM-targeted green fluorescent protein (GFP). We found that mitochondria in contact with the *Toxoplasma* vacuole released large structures that were positive for OMM, which we termed "SPOTs." Analysis of SPOTs in fixed and live cells revealed that SPOTs did not contain proteins of the mitochondrial matrix and inner mitochondrial membrane (IMM).

RESULTS: Having identified *Toxoplasma* infection as a natural stress that induced OMM remodeling and the shedding of SPOTs, we next dissected how these structures are formed. We found that the secreted effector protein TgMAF1 (*Toxoplasma gondii* mitochondrial association factor 1), which tethers the host OMM to the parasite vacuole membrane, was required for SPOT formation. TgMAF1 led to a decrease in the amount of mitochondrial proteins during infection. In particular, the OMM proteins mitofusin 1 and mitofusin 2 were degraded during infection. These proteins, which mediate a nutritional defense against *Toxoplasma* by promoting mitochondrial uptake of fatty acids, localized to SPOTs. The ability of TgMAF1 to induce SPOTs depended on its binding to the host OMM import receptor TOM70 (translocase of the outer membrane 70), whose import function TgMAF1 impaired. TOM70 was required for optimal parasite growth and enabled an interaction between TgMAF1 and the OMM translocase SAM50 (sorting assembly machinery 50 kDa subunit), which is a key component of the OMM-IMM mitochondrial intermembrane space bridging (MIB) complex. The genetic ablation of SAM50 and the overexpression of an OMM-targeted protein induced the formation of SPOT-like structures independently of infection.

CONCLUSION: Because SAM50 is the only component of mitochondrial import machinery that bridges the OMM and IMM, it is in a position to translate OMM stress into the removal of compromised OMM. TgMAF1 behaves as a mitochondrial preprotein that uses the host receptor TOM70 to interact with SAM50. This enables *Toxoplasma* to hijack a cellular response to OMM stress—the formation of SPOTs—and drive the constitutive shedding of the OMM. Consequently, levels of mitochondrial proteins that restrict parasite growth are depleted, and import machinery that is required for mitochondrial biogenesis is sequestered on SPOTs. In an infection-independent context, however, we propose that SPOT-like structures could mitigate OMM stress by enabling the excision of dysfunctional OMM machinery, such as import receptors or translocases during defective import. Our finding that OMM remodeling occurs during infection and infection-independent scenarios sheds light on potential cellular mechanisms that safeguard OMM function. ■

The list of author affiliations is available in the full article online.
*Corresponding author. Email: pernas@age.mpg.de
Cite this article as X. Li *et al.*, *Science* **375**, eabi4343 (2022).
DOI: 10.1126/science.abi4343

READ THE FULL ARTICLE AT
https://doi.org/10.1126/science.abi4343

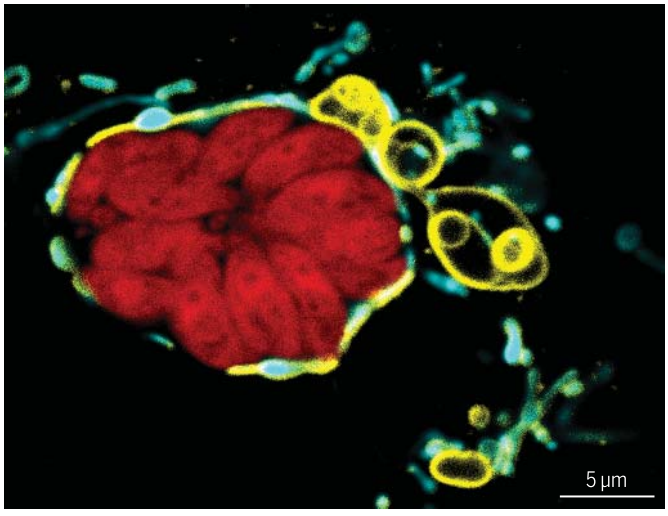

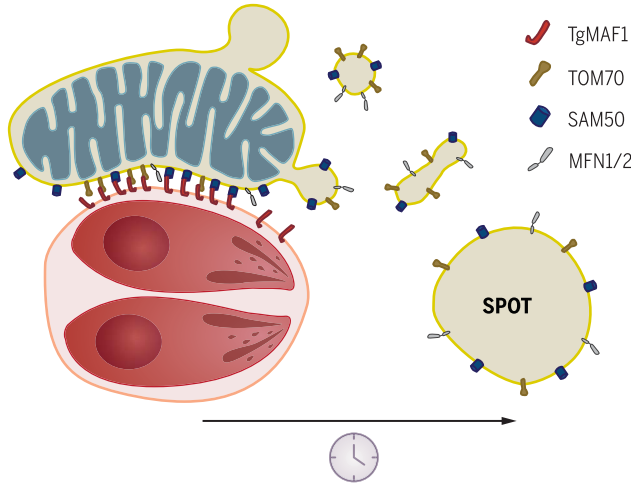

Mitochondria shed SPOTs during *Toxoplasma* infection. (**Left**) Mitochondria surrounding the parasite *Toxoplasma* (red) shed SPOTs, large structures positive for OMM (yellow) that lack mitochondrial matrix (cyan). (**Right**) Cartoon depiction of image at left as infection progresses (clock). OMM proteins—including the import translocase SAM50, and MFN1 and MFN2, which are required for mitochondrial fusion—are sequestered on SPOTs.

RESEARCH ARTICLE

CELL BIOLOGY

Mitochondria shed their outer membrane in response to infection-induced stress

Xianhe Li[1], Julian Straub[1], Tânia Catarina Medeiros[1], Chahat Mehra[1], Fabian den Brave[2], Esra Peker[3], Ilian Atanassov[1], Katharina Stillger[3], Jonas Benjamin Michaelis[4], Emma Burbridge[5,6], Colin Adrain[5,6], Christian Münch[4], Jan Riemer[3,7], Thomas Becker[2], Lena F. Pernas[1,7]*

The outer mitochondrial membrane (OMM) is essential for cellular homeostasis. Yet little is known of the mechanisms that remodel it during natural stresses. We found that large "SPOTs" (structures positive for OMM) emerge during *Toxoplasma gondii* infection in mammalian cells. SPOTs mediated the depletion of the OMM proteins mitofusin 1 and 2, which restrict parasite growth. The formation of SPOTs depended on the parasite effector TgMAF1 and the host mitochondrial import receptor TOM70, which is required for optimal parasite proliferation. TOM70 enabled TgMAF1 to interact with the host OMM translocase SAM50. The ablation of SAM50 or the overexpression of an OMM-targeted protein promoted OMM remodeling independently of infection. Thus, *Toxoplasma* hijacks the formation of SPOTs, a cellular response to OMM stress, to promote its growth.

Mitochondria are dynamic organelles that coordinate cellular functions essential for life, including diverse metabolic processes, cell division and differentiation, and immune signaling (*1*). At the interface between mitochondria and the rest of the cell, the outer mitochondrial membrane (OMM) plays a central role in all mitochondrial functions. Arguably, the most vital of these functions is to enable mitochondrial biogenesis by providing a platform for the machinery that imports almost all ~1200 nuclear-encoded mitochondrial proteins in mammals (*2*). Dysfunction of the mitochondrial import machinery results in systemic pathology of the organelle and organismal death (*3*). Because all mitochondrial functions rely on the import of proteins into the organelle, quality control pathways must regulate import processes and prevent the toxic accumulation of nonimported or mislocalized precursor proteins, several of which have been identified and studied in yeast (*4*). By contrast, how the OMM is protected and remodeled during import stress in mammals is largely uncharacterized.

Intracellular microbes pose a naturally occurring threat to mitochondria, which is perhaps the evolutionary consequence of the role that these organelles play in antimicrobial immune signaling and nutritional defense (*5*–*8*). Several bacteria, for example, release effector proteins that localize to the OMM and perturb mitochondrial function (*9*). We used the parasite *Toxoplasma gondii*, which infects up to one-third of the human population and has an unparalleled host range, to investigate the cellular responses that remodel the OMM (*10*). With respect to the OMM, *Toxoplasma* is of particular interest because it is one of several pathogens to reside in vacuoles found in close physical proximity to mitochondria (*11*, *12*).

[1]Max Planck Institute for Biology of Ageing, Cologne, Germany. [2]Institute of Biochemistry and Molecular Biology, Medical Faculty, University of Bonn, Bonn, Germany. [3]Institute of Biochemistry, University of Cologne, Cologne, Germany. [4]Institute of Biochemistry II, Faculty of Medicine, Goethe University, Frankfurt am Main, Germany. [5]Patrick G Johnston Centre for Cancer Research, Queen's University Belfast, Belfast, Northern Ireland. [6]Instituto Gulbenkian de Ciência, Oeiras, Portugal. [7]Cologne Excellence Cluster on Cellular Stress Responses in Aging-Associated Diseases (CECAD), University of Cologne, Cologne, Germany.
*Corresponding author. Email: pernas@age.mpg.de

Mitochondria shed SPOTs during *Toxoplasma* infection

To monitor the impact of *Toxoplasma* infection on the OMM, we infected mouse cells stably expressing enhanced green fluorescent protein (eGFP) fused to the OMM-targeting transmembrane (TM) domain of OMP25 (OMM-GFP) with mCherry-expressing *Toxoplasma* (*13*). As early as 6 hours after infection, we observed large spherical and elliptical structures enriched for OMM-GFP that were absent in uninfected cells, which we termed "SPOTs" (structures positive for outer mitochondrial membrane) (Fig. 1A). The percentage of SPOT-positive cells increased over the course of infection (Fig. 1B). At 24 hours after infection, >50% of infected cells contained between 1 and 20 SPOTs that were on average ~2.6 μm in diameter (Fig. 1, A to D). To exclude the possibility that the formation of SPOTs depended on OMM-GFP expression, we also examined infected cells using a fluorescent phosphatidylcholine conjugate (FL-HPC) that in part integrates into mitochondrial membranes. In both wild-type (WT) and OMM–BFP (blue fluorescent protein)–expressing U2OS (human) cells, FL-HPC distributed to SPOT-like structures that were only present in infected cells (fig. S1). Thus, SPOT formation is a general consequence of *Toxoplasma* infection in mammalian cells.

Despite their large size, we suspect that SPOTs have been overlooked because although they retain OMM proteins such as TOM20 (translocase of the outer membrane 20), they are not labeled by mitotracker, a commonly used vital dye that accumulates in mitochondria in a membrane potential–dependent manner (Fig. 1, E to F, and figs. S1 and S2A). Furthermore, in live-cell imaging experiments, SPOTs also lack fluorescent markers of other mitochondrial compartments, including the matrix and inner mitochondrial membrane (IMM) (Fig. 1, G to J). We confirmed that SPOTs also lacked endogenous levels of proteins of the intermembrane space (IMS) (AIFM1), IMM (ATPF1B), and matrix (CS and mtHSP70) (fig. S2, B to E). Thus, the OMM is remodeled to release SPOTs during *Toxoplasma* infection. Hereafter, we refer to SPOTs as structures that are positive for an OMM marker but that lack markers of other mitochondrial compartments.

The large diameter and lack of mitochondrial matrix proteins in SPOTs suggested that they differed from fragmented mitochondria as well as mitochondria-derived compartments (MDCs) and mitochondria-derived vesicles (MDVs), which form in response to amino acid toxicity and oxidative stress, respectively (*14*–*19*). MDCs average 1 μm in diameter and depend on the OMM guanosine triphosphatase (GTPase) MIRO1 (mitochondrial rho GTPase 1), which mediates mitochondrial trafficking (*16*, *17*). The smaller MDVs that transport cargo between mitochondria and peroxisomes or lysosomes—the latter of which depend on the E3 ligase parkin and the mitochondrial kinase PINK1 (PTEN-induced putative kinase protein 1)—range between 75 and 150 nm in diameter (*14*, *18*, *20*). Neither the loss of the key mitochondrial fission factor DRP1 (dynamin-related protein 1) nor of MIRO1 and its paralog MIRO2 significantly affected SPOT formation during infection (fig. S3). Moreover, SPOTs also formed during infection in HeLa cells that were deficient for PINK1 in a manner similar to that of WT HeLa cells that lacked detectable parkin expression (fig. S4) (*21*).

The dynamin-binding partner SNX9 (sorting nexin 9) that remodels endocytic membranes mediates the emergence of a subset of MDVs that contain the matrix proteins OGDH (oxoglutarate dehydrogenase) and mtHSP70 (*22*–*24*). We thus asked whether SNX9 also participated in SPOT formation. In infected cells, the depletion of SNX9 prevented the formation of SPOTs (fig. S5, A to E). However, *Toxoplasma*-induced SPOTs lacked both mtHSP70 and OGDH, matrix proteins that are markers of SNX9-dependent MDVs (figs. S2E and S5F). Thus, SPOTs represent an independent class of structures that bud from the OMM.

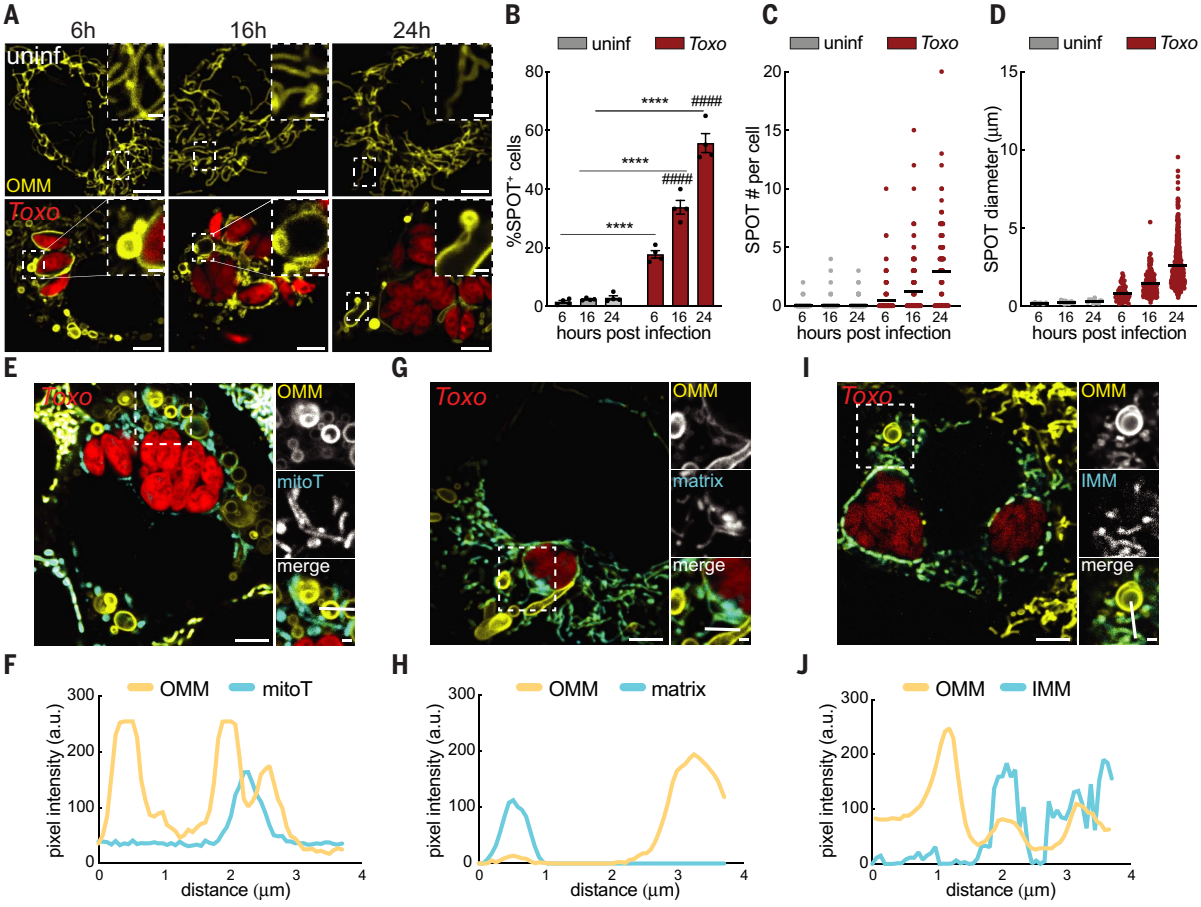

Fig. 1. The outer membrane is remodeled during *Toxoplasma* infection through the release of SPOTs. (**A**) Representative live-cell images of the OMM (GFP) in uninfected (uninf) and *Toxoplasma* (mCh)–infected (*Toxo*) MEFs at 6, 16, and 24 hours after infection. (**B**) Percentage of SPOT-positive cells in experiments as in (A); data are mean ± SEM of more than 100 cells counted from four biological replicates; ****P < 0.0001 for uninfected versus infected; ####P < 0.0001 for 6 hours after infection versus 16 and 24 hours after infection by means of two-way ANOVA. (**C** and **D**) Scatterplot with mean (C) number and (D) diameter of SPOTs in experiments as in (A) from more than 30 infected cells from three biological replicates. (**E**, **G**, and **I**) Representative live-cell images of the OMM (GFP) in *Toxoplasma* (mCherry)–infected MEFs (E) labeled with MitoTracker Deep Red (mitoT); (G) expressing matrix-targeted BFP (matrix); or (I) expressing RFP-tagged TIM50 (IMM). (**F**, **H**, and **J**) Corresponding pixel intensity plots for white line in (E), (G), and (I) insets, respectively. Scale bars, 5 µm and (insets) 1 µm.

The parasite effector TgMAF1 is required for SPOT formation and the depletion of host mitochondrial proteins

How does *Toxoplasma* induce the formation of SPOTs? In live-cell imaging analyses of infected cells, SPOTs were readily visualized emerging from mitochondria in proximity to the parasite vacuole (PV) (Figs. 1, A, E, G, and 2A and movies S1 and S2). At the mitochondria-*Toxoplasma* interface, the OMM is tethered to the PV membrane (PVM) at a distance of 12 to 17 nm, regions that can be referred to as "contact sites," a term that describes areas of close membrane apposition between organelles (*25*, *26*). Mitochondria-*Toxoplasma* PV contact sites, previously termed host mitochondrial association (HMA), are completely dependent on the parasite effector protein TgMAF1 (*Toxoplasma gondii* mitochondrial association factor 1) (*27*). TgMAF1 is anchored in the PVM and posited to interact with host mitochondria through its cytosolically exposed C terminus (*27*–*29*). TgMAF1 affects the host inflammatory responses during infection, but its function at mitochondria-*Toxoplasma* contact sites remains elusive (*27*). To test the hypothesis that TgMAF1 tethering of host mitochondria contributes to SPOT formation, we assessed the frequency of SPOTs in cells infected with WT or Δ*maf1* parasites. The ablation of TgMAF1 completely prevented the formation of SPOTs (Fig. 2, B to E). Thus, TgMAF1 is required for the formation of SPOTs during infection.

The physical remodeling of the OMM during *Toxoplasma* infection prompted us to ask whether the formation of SPOTs also led to changes in its composition. To address this, we used proteomics to compare the protein abundances between whole cell extracts and mitochondria immunopurified (mitoIP) from uninfected cells and cells infected with WT or Δ*maf1* parasites (*13*). Infection with WT parasites caused a global decrease in the whole cell and mitoIP abundance of mitochondrial proteins that was partially prevented during infection with Δ*maf1* parasites (Fig. 3, A to D; fig. S6, A to D; and data files S1 and S2). Thus, TgMAF1, beyond its tethering function, is also required for the decrease in mitochondrial proteins during infection.

A targeted analysis of changes in the OMM compartment from which SPOTs are derived revealed TgMAF1-dependent decreases in several proteins that mediate antimicrobial defense, including MIRO1, MIRO2, mitofusin 1 (MFN1), and MFN2, results we confirmed with immunoblotting (Fig. 3, E to F) (*5*, *30*). The depletion of MFN1 and MFN2 during infection was particularly intriguing given that these OMM GTPases are essential for mitochondria to restrict parasite proliferation and raised the question of how TgMAF1 drove their decrease (*5*). Infection did not reduce *MFN1* and *MFN2* mRNA amounts (fig. S7A). Furthermore, neither the loss of PINK1, a key

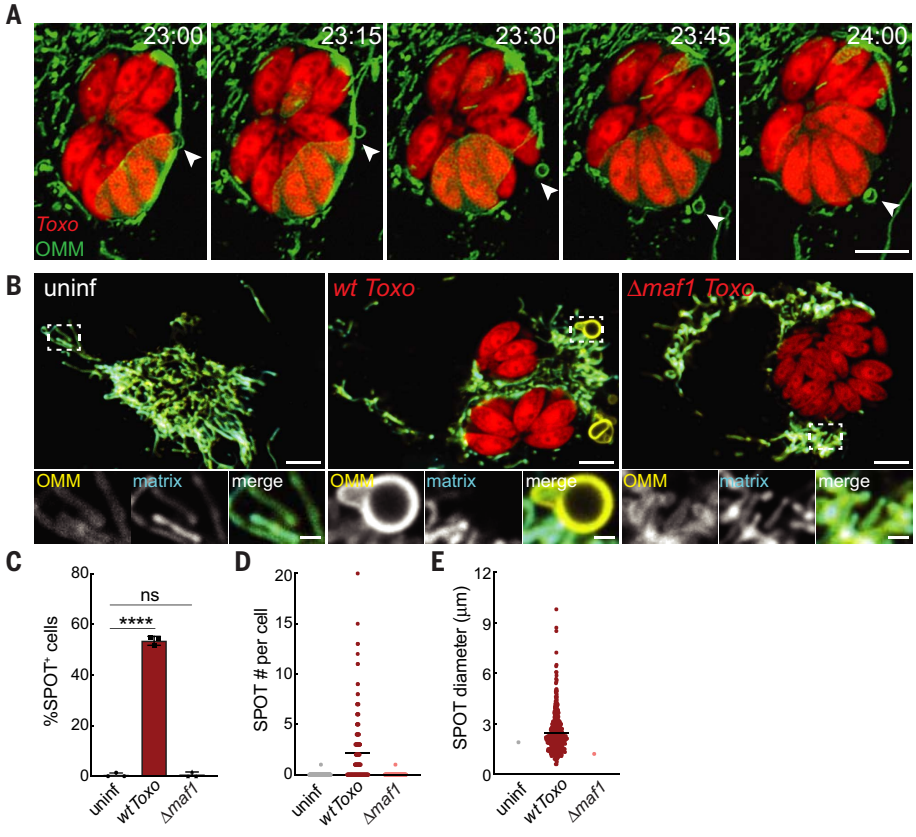

Fig. 2. TgMAF1 is required for SPOT formation. (**A**) Representative live-cell images of the OMM (GFP) in *Toxoplasma* (mCh)–infected HFFs. Shown is the formation of a SPOT (indicated with white arrowhead) over a 1-hour time-lapse movie starting at 23 hours after infection with frames captured every 15 min (movie S2). Scale bar, 5 μm. (**B**) Representative live-cell images of the OMM (GFP) and matrix (BFP) in uninf, WT *Toxo* (mCh)–infected, or Δ*maf1 Toxo* (mCh)–infected U2OS cells. Scale bars, 5 μm and (inset) 1 μm. (**C**) Percentage of SPOT-positive cells in experiments as in (B). Data are mean ± SEM of more than 100 cells counted from three biological replicates. ns, not significant; ****$P < 0.0001$ for uninfected versus infected by means of one-way ANOVA analysis. (**D** and **E**) Scatterplots with mean (D) number and (E) diameter of SPOTs in experiments as in (B) from more than 30 infected cells from three biological replicates.

mediator of mitophagy, nor the loss of the essential autophagy gene *Atg7* prevented the *Toxoplasma*-induced reduction in MFN1 and MFN2 (fig. S7, B and C). The decrease in MFN1 and MFN2 correlated with their redistribution from mitochondria to SPOTs that were also positive for FAF2 (Fas-associated factor family member 2), a protein that recruits the proteasomal machinery required for endoplasmic reticulum (ER)–associated degradation (Fig. 3, G to J, and fig. S7, D to F) (*31*). Because MFN1 and MFN2 are regulated by the ubiquitin/proteasome system (UPS) and FAF2 mediates the turnover of MFN1/2 (Fzo1) in yeast, we asked whether FAF2 played such a role in our system (*32*, *33*). In mouse embryonic fibroblasts (MEFs) in which FAF2 was ablated (FAF2 KO MEFs), the depletion of MFN1 and MFN2 in mitochondrial and whole-cell fractions that would normally be caused by infection was prevented (fig. S7G). Conversely, the expression of *Faf2* cDNA in FAF2 KO MEFs rescued their depletion during infection (fig. S7H). To test a potential role for the UPS in mediating the degradation of MFN1 and MFN2, we turned to TAK-243, a small molecular inhibitor of the ubiquitin activation step that precedes degradation by the UPS because inhibitors of proteasomal machinery restrict parasite proliferation (fig. S7, I to J) (*34*). Treatment with TAK-243 did not affect parasite burden as assessed by *Toxoplasma* TgGAP45 but prevented the depletion of MFN1 and MFN2 and to a lesser extent that of MIRO1 and MIRO2, which also localized to SPOTs during infection (figs. S7, I to J, and S8). Thus, FAF2 mediates the proteolytic degradation of MFN1 and MFN2 on SPOTs, and certain OMM proteins that localize to SPOTs are targeted by the UPS for degradation.

TgMAF1 inhibits host TOM70 import function

How does TgMAF1 induce the remodeling of the OMM into SPOTs? We reasoned that identifying TgMAF1-interacting factor(s) might provide clues to host proteins involved in SPOT formation. To find these host factors, we immunopurified TgMAF1 from cells infected with Δ*maf1* parasites complemented with a hemagglutinin (HA)–tagged TgMAF1 (Δ*maf1:HA-MAF1*) at a multiplicity of infection (MOI) of 1, 2.4, and 6 and identified the major interaction partners using mass spectrometry. The OMM import receptor TOM70 was the most abundant host protein found at >256-fold enrichment in TgMAF1-IPs of cells infected at all MOIs relative to control IPs (Fig. 4A and data file S3). TOM70 is required for *Toxoplasma* association with host mitochondria and is enriched on mitochondria tethered to the PV (*35*). To confirm that parasite TgMAF1 and host TOM70 interact during infection, we also performed an immunoblot analysis of TgMAF1-IPs. TgMAF1 coimmunoprecipitated TOM70 but not other OMM proteins, including VDAC1 (voltage-dependent anion channel 1) or VDAC2, nor its putative interacting partner HSPA9 (heat shock protein family A member 9) (Fig. 4B) (*35*). Furthermore, stably expressed GFP-tagged TOM70 coimmunoprecipitated TgMAF1 from lysates of infected MEFs and was enriched on the OMM of a mitochondrion tethered to the PV at 20-fold higher concentrations than those of OMM regions of the same mitochondrion not in contact with the PV (Fig. 4, C to E). This consequence of infection was completely dependent on TgMAF1 because the distribution of TOM70 did not differ between cells infected with Δ*maf1:HA* parasites and uninfected cells (Fig. 4, D to E). To address whether TgMAF1 and TOM70 directly interact, we incubated TgMAF1 produced in a cell-free system with the purified cytosolic domain of yeast TOM70. Only full-length TgMAF1—but not a mutant lacking a predicted internal mitochondrial targeting sequence (iMTS), which mediates precursor binding to TOM70—bound to affinity-purified TOM70 (Fig. 4, F to G) (*35*, *36*). Thus, parasite TgMAF1 and host TOM70 directly interact during infection.

TOM70 has two critical functions at the OMM. First, TOM70 recruits cytosolic chaperones such as HSP90 that mediate precursor import and thus protects against proteotoxicity owing to accumulated precursors through its N-terminal CLAMP domain (*37*, *38*). Second, TOM70 is a major import receptor, most notably for SLC25 mitochondrial carriers that it binds through its CORE and C-tail domains (*38*). Thus, TgMAF1 could perturb TOM70 chaperone-binding activity or import activity to exploit a host response to import stress, leading to SPOT formation. To address these possibilities, we asked whether the abundances of HSP90 or SLC25 proteins were altered in our proteomics datasets of uninfected cells and cells infected with WT or Δ*maf1* parasites (Fig. 3, A to D). The levels of HSP90 were increased in mitoIPs in a

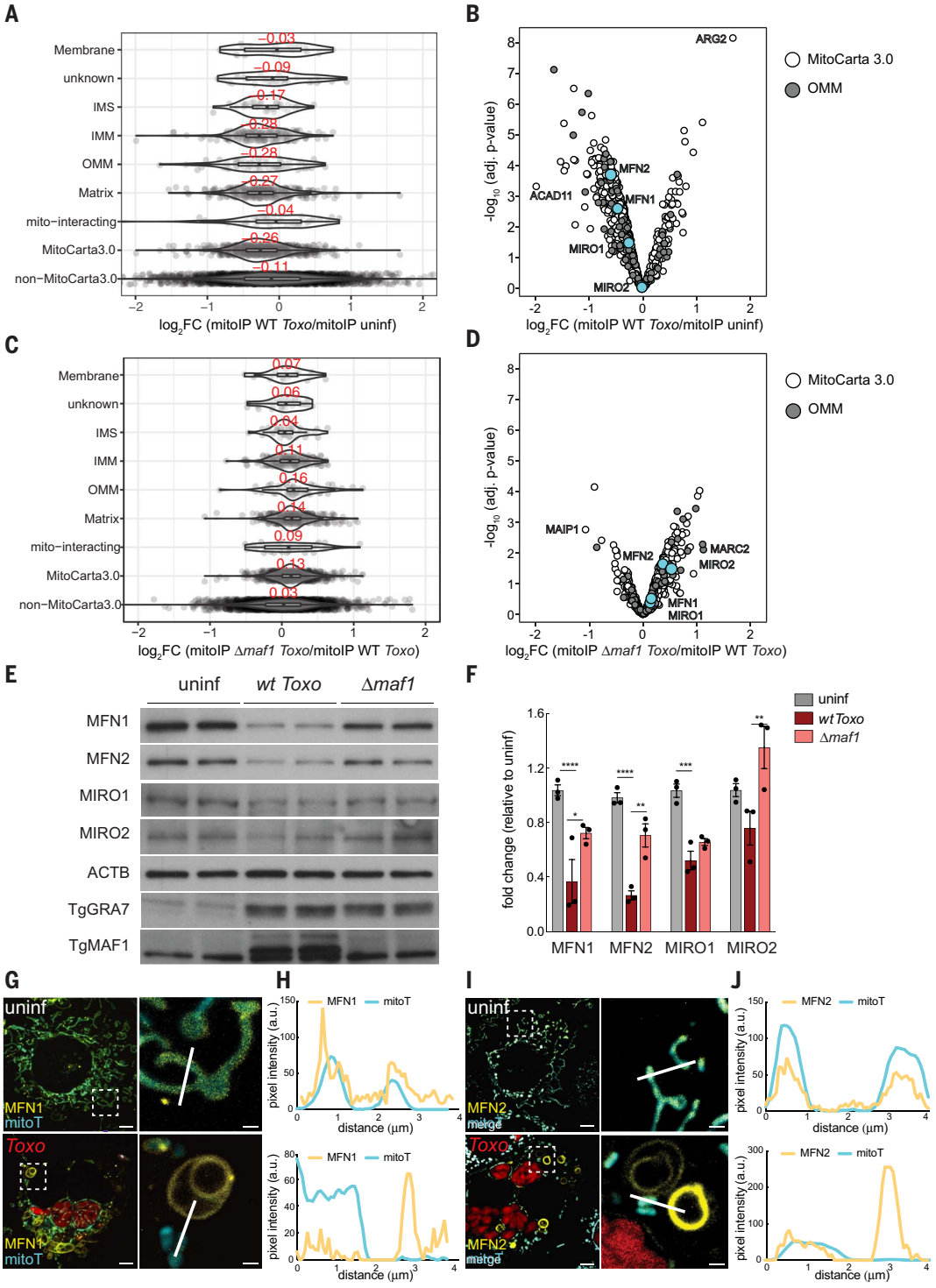

Fig. 3. TgMAF1 drives changes in the mitochondrial proteome and the depletion of certain OMM proteins that localize to SPOTs. (**A** and **C**) Mitochondria were immunopurified (mitoIP) from HeLa cells that were uninfected (uninf) (n = 4), WT *Toxo*-infected (n = 4), or Δ*maf1 Toxo*–infected (n = 3) at 24 hours after infection and analyzed by means of mass spectromtery. Shown are boxplots depicting the $\log_2$-fold change (FC) of detected MitoCarta3.0 proteins between indicated treatments according to submitochondrial localization. Median values for each subcompartment are indicated in red. (**B** and **D**) Volcano plot of proteins in (A) and (C). Dark gray, OMM proteins as classified by MitoCarta3.0; white, all other MitoCarta3.0 proteins. (**E**) Cells were uninf, WT *Toxo*–, or Δ*maf1*-infected for 24 hours and analyzed by means of immunoblotting for MFN1, ~80 kda; MFN2, ~80 kDa; MIRO1, ~75 kDa; MIRO2, ~75 kDa; ACTB, ~45 kDa; TgGRA7, ~32 kDa; and TgMAF1, ~60 kDa. (**F**) Fold change in density of protein bands imaged as in (E) normalized to actin and relative to mean of uninfected samples. Data are mean ± SEM from three biological replicates; $^{*}P < 0.05$, $^{**}P < 0.01$, $^{***}P < 0.001$, $^{****}P < 0.0001$ for WT *Toxo* versus uninfected or Δ*maf1*-infected samples. Representative live-cell images of (**G**) *Mfn1*$^{-/-}$*:GFP-Mfn1* MEFs and (**I**) *Mfn2*$^{-/-}$ MEFs expressing mCh-MFN2 at 24 hours after infection with *Toxoplasma* (BFP). (**H** and **J**) Corresponding pixel intensity plots for white line in (G) and (I) insets, respectively. Scale bars, 5 μm and (inset) 1 μm.

TgMAF1-dependent manner (fig. S9, A and B). Opposite to HSP90 however, concentrations of 11 of the 22 detected SLC25 proteins were decreased in a MAF1-dependent manner, hinting at an impact of MAF1 on TOM70-dependent import (fig. S9, A to B). To more carefully dissect how TgMAF1 affects TOM70 import function, we turned to budding yeast, a workhorse for mitochondrial import studies and a system in which TOM70 function is well characterized (*36*, *37*). After confirming that stably expressed TgMAF1 coimmunoprecipitated yeast TOM70, we assessed its effect on TOM70 import (fig. S9C). Mitochondria isolated from TgMAF1^{+} yeast imported the TOM70-dependent precursor AAC (ADP/ATP carrier) more slowly than did mitochondria from WT yeast, whereas the Su9–DHFR (dihydrofolate reductase) fusion protein, which does not require TOM70, was imported at similar rates (fig. S9, D to G) (*37*, *39*). Furthermore, TgMAF1 stably expressed in mammalian cells coimmunoprecipitated TOM70 and impaired the import of AAC2 in a TOM70-dependent manner (Fig. 4, H to K). Thus, TgMAF1 negatively affects TOM70-dependent import.

Host TOM70 and SAM50 are required for infection-induced SPOT formation

To further explore a potential link between TOM70 inhibition and SPOT formation, we asked whether the expression of TgMAF1 alone—which was sufficient to impair TOM70-dependent import—also induced the formation of SPOTs. However, neither TgMAF1, which localizes to host mitochondria when expressed in mammalian cells, nor an ER-anchored TgMAF1 remodeled the OMM in a manner reminiscent of *Toxoplasma*-induced SPOTs, indicating a requirement for other parasite factors in their formation (fig. S10) (*27*). To test the impact of a more complete loss of TOM70 function, we generated cells lacking TOM70 (Fig. 5A). Contrary to our expectation, the loss of TOM70 did not induce SPOT formation but instead prevented their formation during infection (Fig. 5, B to E), whereas HSP90 inhibition with the specific inhibitor 17-DMAG (17-dimethylaminoethylamino-17-demethoxygeldanamycin) did not affect the rate of their formation (fig. S11). We also noticed that the loss of TOM70 impaired the growth of TgMAF1^{+} but not Δ*maf1* parasites (Fig. 5F). Thus, we considered an alternate scenario in which *Toxoplasma* exploits host TOM70 to mediate the import of TgMAF1 into host mitochondria through an OMM translocase. Because TgMAF1 is anchored into the PVM, its stable interaction with OMM import machinery would be sensed as a chronic stress, activating a host response that remodels the OMM through the budding of SPOTs. The constant formation of SPOTs, however, would lead to the shedding of OMM proteins, including import machinery and MFN1 and MFN2, which restrict parasite growth (Fig. 5G) (*5*). To test whether a TgMAF1-TOM70 interaction was critical for SPOT formation, we generated Δ*maf1* parasites expressing a TgMAF1 mutant that exhibits a diminished interaction with TOM70 because of a trio of basic residues at its C terminus (TgMAF1^{RKK}) (fig. S12, A to B) (*35*). Cells infected with Δ*maf1:MAF1*^{RKK} mutant parasites were SPOT-less, despite retaining a significant capacity to tether mitochondria to the PVM (figs. S12, C to F, and S13, A and B). Thus, a stable TgMAF1-TOM70 interaction is essential for the formation of SPOTs.

Because the loss of TOM70 did not form SPOTs, we posited that the stress required for their formation was derived from a TOM70-dependent interaction between MAF1 and another OMM host import factor (Fig. 5G). In line with this possibility, a study of TgMAF1 interactors has identified SAM50 (sorting assembly machinery 50 kDa subunit), a translocase that is essential for the OMM integration of a subset of mitochondrial proteins, and MIC19 and MIC60, proteins with which SAM50 forms the OMM-IMM mitochondrial intermembrane space bridging (MIB) complex (*29*, *40*). We therefore asked whether TOM70 was required for a TgMAF1-SAM50 interaction. SAM50 was present in TgMAF1-IPs from infected WT cells but not cells in which TOM70 was deleted (Fig. 6A). We obtained similar results for MIC19 and MIC60 (Fig. 6A). Thus, TOM70 is required for TgMAF1 to interact with the OMM translocase SAM50 and its interacting partners MIC60 and MIC19.

SAM50 is the only component of host mitochondrial import machinery with a defined role in bridging the OMM and IMM. We thus reasoned that TgMAF1 could induce the formation of SPOTs that are OMM-positive but lack IMM by exerting an effect on SAM50. SAM50, but not its MIB-complex partner MIC60 that is tethered to the IMM, was enriched on SPOTs in infected cells (Fig. 6B and fig. S14). To directly test the possibility that SPOTs resulted from a separation of the OMM and IMM, we used cell lines in which the MIB components *SAM50* and *MIC60* as well as *TOM70* were silenced with doxycycline-inducible short hairpin RNA (shRNA). We confirmed that TOM70 is required for SPOT formation (Fig. 6, C to F). The depletion of *SAM50* was sufficient to induce smaller SPOT-like structures in >25% of uninfected cells relative to <1% of cells expressing a control shRNA (Fig. 6, C to F). Infection-induced SPOT formation in *SAM50*-deficient cells was blunted (Fig. 6, C to F). Furthermore, we observed minimal differences in the size and number of SPOT-like structures between uninfected and infected *SAM50*-depleted cells. Mitochondria-*Toxoplasma* contact sites were unaffected by the loss of *SAM50* (Fig. 6, C to F, and fig. S13). Similar results were obtained in cells depleted of MIC60 (Fig. 6, C to F, and fig. S13). To further test the possibility that SPOTs result from the separation of the OMM and IMM, we generated cells that stably express BFP fused to a tether that bridges the OMM and IMM (O-I$_t$) (*41*). Expression of the O-I$_t$ significantly decreased the rate of formation of SPOTs. In addition, the average number of SPOTs per cell and their diameter were decreased relative to cells that express matrix-targeted BFP during infection (Fig. 6, I to J). Thus, *Toxoplasma* induces SPOTs in a SAM50-dependent manner, and the loss of SAM50 is sufficient to induce the formation of SPOT-like structures in the absence of infection.

Import-linked OMM stress induces OMM shedding independently of infection

If the remodeling of the OMM that occurs during infection represents a general response to import stress, we expected to see the formation of SPOT-like structures upon perturbation of import independently of infection, such as by the overexpression of an OMM protein. To this end, we isolated cells that express the GFP-tagged OMM-targeting α-helical TM of OMP25 at >20-fold times; greater (OMM^{hi}) than that in cells used in prior experiments (OMM^{lo}) and that slowed cell proliferation (fig. S15, A and B). We observed a substantial remodeling of the OMM in >20% of OMM^{hi} cells but not in OMM^{lo} cells, despite the overexpression of matrix-BFP in both cell lines (fig. S15, C to F). This indicated a link between stress related to the import of OMM proteins and the formation of SPOT-like structures. No remodeling of the OMM was observed after treatment with the protonophore CCCP (carbonyl cyanide m-chlorophenyl hydrazone), which dissipates mitochondrial membrane potential (MMP) and prevents the import of presequence-containing proteins, or MitobloCK6, which inhibits the IMS import pathway (fig. S16) (*42*). We next generated cells in which we expressed GFP fused to an artificial clogger of the TOM40 channel that forms the entry gate for almost all mitochondrial proteins other than α-helical OMM proteins (fig. S17A). The clogger contains DHFR between a cytochrome b_2 presequence that directs it to the IMM by way of the TOM complex and a heme binding domain that slows its import (fig. S17A) (*43*). The addition of methotrexate (MTX) that stabilizes the folding state of DHFR leads to its arrest at the TOM complex and further accumulation in the cytosol, as we observed (fig. S17) (*43*, *44*). However, the expression of the clogger with vehicle or MTX did not lead to SPOT formation (fig. S17, C to F). Thus, the OMM is remodeled after stress linked to the overexpression of an α-helical OMM protein

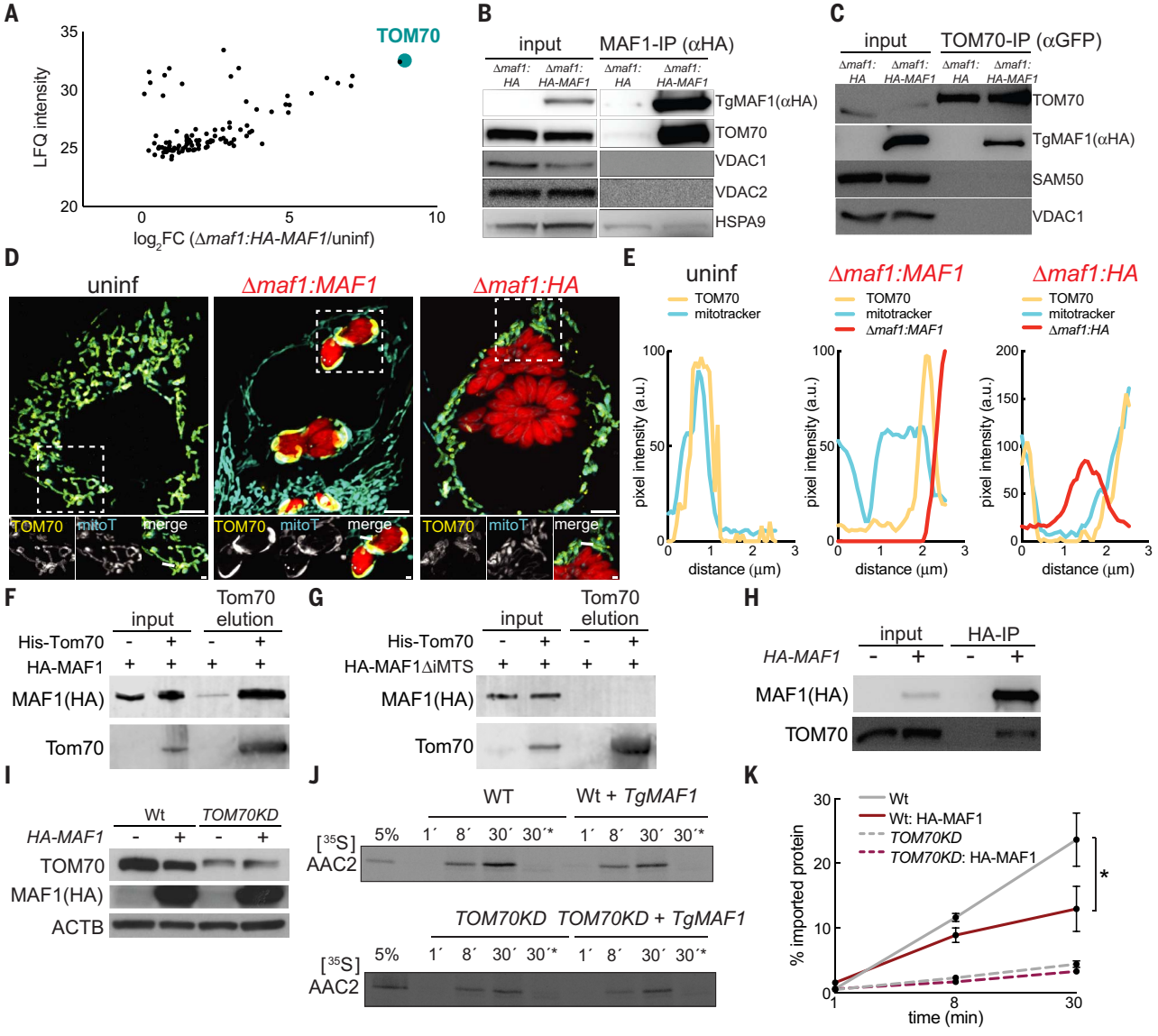

Fig. 4. TgMAF1 binds the host receptor TOM70 and inhibits its import function. (**A**) Anti-HA immunoprecipitates (IPs) from cells that were mock-infected (uninf) or infected with Δ*maf1*:HA-MAF1 parasites at an MOI of 1, 2.4, and 6 and analyzed by means of mass spectrometry; data for MOI 2.4/uninf are shown for 101 human protein hits that had a positive log_2FC for the comparisons: all MOIs/uninf, MOI:6/MOI:2.4, MOI:6/MOI:1, MOI:2.4/MOI:1. LFQ, label-free quantification. (**B**) Anti-HA IPs from U2OS cells infected with Δ*maf1*:HA or Δ*maf1*:HA-MAF1 parasites and analyzed by means of immunoblotting (IB) for TgMAF1, ~60 kDa; HSPA9, ~90 kDa; VDAC1, ~34 kda; VDAC2, ~34 kda; TOM70, ~72 kDa. (**C**) Anti-GFP IPs from TOM70-GFP–expressing MEFs 24 hours after infection with Δ*maf1*:HA or Δ*maf1*:HA-MAF1 and analyzed by means of IB for indicated proteins: TOM70-GFP, ~105 kDa; TgMAF1, ~60 kDa; SAM50, ~55 kda; VDAC1, ~34 kda. (**D**) Representative live-cell images of mitoT-labeled TOM70-GFP MEFs at 24 hours after mock infection (uninf) or infection with Δ*maf1:HA-MAF1* or Δ*maf1:HA* parasites. Scale bars, 5 μm and (inset) 1 μm. (**E**) Corresponding pixel intensity plots for white line in (D) inset. (**F**) HA-MAF1 and (**G**) HA-MAFΔiMTS were incubated with his-tagged TOM70 (cytosolic domain) and subjected to affinity purification with Ni-NTA agarose. Input and elution were analyzed by means of IB. (**H**) HA-IPs from MEFs expressing HA-MAF1 and analyzed by means of IB for TOM70, ~72 kDa, and HA-MAF1, ~60 kDa. (**I**) IB analyses of lysates from WT and TOM70-suppressed 293Ts ± HA-MAF1 cDNA: TOM70, ~72 kDa; HA-MAF1, ~60 kDa. (**J**) [^{35}S]AAC2 import into mitochondria isolated from cells in (I) at indicated times was analyzed by means of SDS–polyacrylamide gel electrophoresis (SDS-PAGE) and autoradiography. Nonimported proteins were removed through proteinase K treatment; asterisk indicates CCCP treatment. (**K**) Signals in (J) were quantified, and the amount of imported protein relative to input (5%) was plotted. Data are mean ± SEM from three biological replicates, *$P < 0.05$ for WT versus WT:HA-MAF1 by means of two-way ANOVA analysis.

but not depolarization of the MMP, inhibition of the IMS pathway, or clogging of the TOM40 channel.

Whether mitochondria are physically remodeled during physiologically occurring stress at the OMM has been unclear. Here, we describe the discovery of SPOTs, a mechanism of OMM remodeling during *Toxoplasma* infection. We propose that *Toxoplasma* coopts the host TOM70 receptor and SAM50 translocase to promote its insertion into the OMM (Fig. 6K). This enables *Toxoplasma* to hijack a host response to OMM stress (Fig. 6K). During import stress independent of infection, the formation of SPOT-like structures could safeguard OMM function by sequestering defective import machinery, preventing the accumulation of precursors and misfolded proteins at

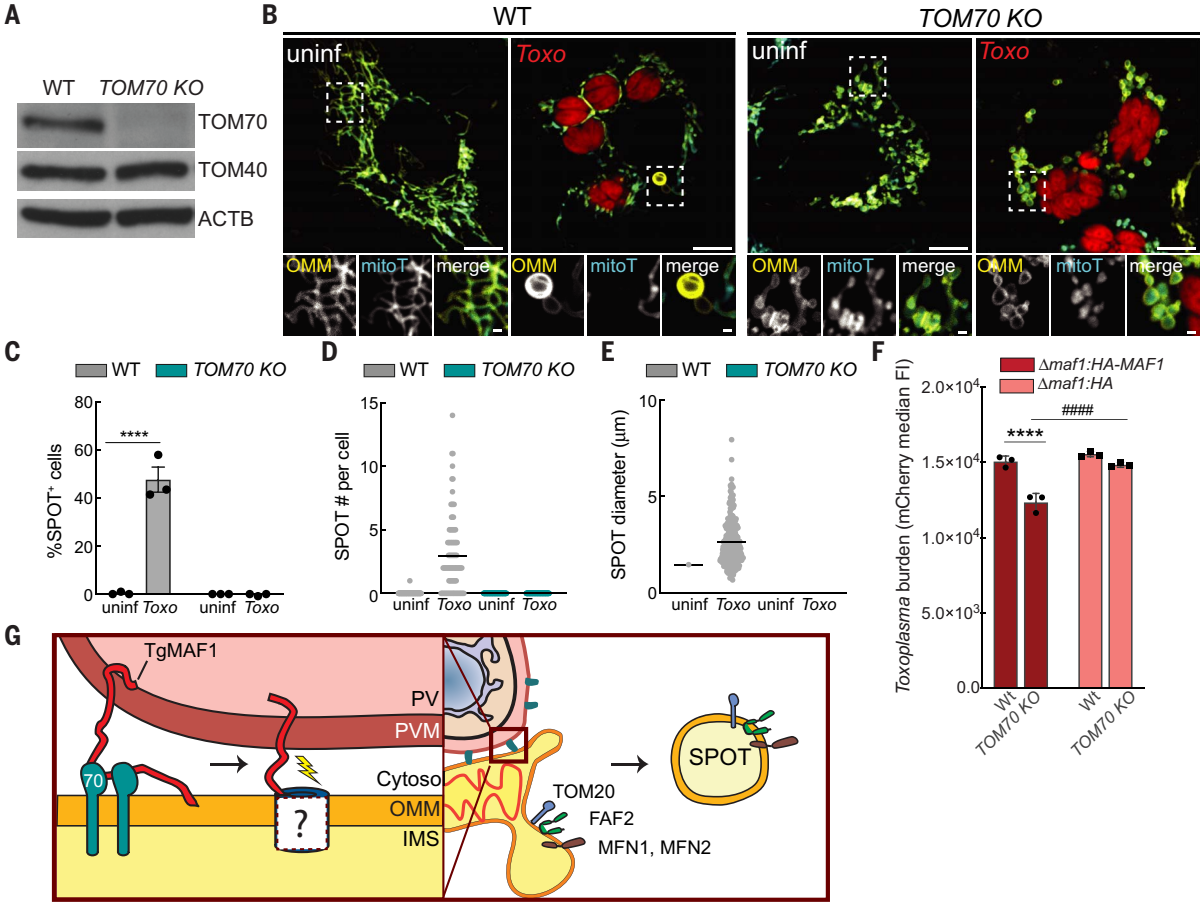

Fig. 5. TOM70 is required for SPOT formation and MAF1-dependent growth. (**A**) WT and *TOM70*-deleted (*TOM70 KO*) HeLas were analyzed by means of immunoblotting for TOM70, ~72 kDa; TOM40, ~40 kDa, and ACTB, ~45 kDa. (**B**) Representative live-cell images of the OMM (GFP) in uninfected (uninf) and *Toxoplasma* (mCh)–infected (*Toxo*)WT and *TOM70 KO* HeLas labeled with mitoT. Scale bars, 5 µm and (inset) 1 µm. (**C**) Percentage of SPOT-positive cells in experiments as in (B). Data are mean ± SEM of more than 100 cells counted from three biological replicates; ****P < 0.0001 for uninfected versus infected by means of two-way ANOVA analysis. (**D** and **E**) Scatterplots with mean (D) number and (E) diameter of SPOTs in experiments as in (B) from more than 30 infected cells from three biological replicates. (**F**) WT and *TOM70 KO* HeLas were infected with *Δmaf1:HA-MAF1* or *Δmaf1:HA* parasites, rinsed at 2 hours after infection, and analyzed 24 hours after infection by means of flow cytometry for *Toxoplasma* burden [red fluorescent protein (RFP) median FI]. Data are mean ± SEM of three biological experiments, ****P < 0.0001 for WT versus *TOM70 KO*, ####P < 0.0001 for *Δmaf1:HA_MAF1* versus *Δmaf1:HA* by means of two-way ANOVA analysis. (**G**) Cartoon model of SPOT formation. Host TOM70 mediates insertion of TgMAF1 into host mitochondria through a hypothetical OMM translocase-insertase inducing a stress that leads to SPOT formation and sequestration of import machinery (TOM20) as well as proteins such as FAF2, MFN1, and MFN2 on SPOTs. PV, parasite vacuole; PVM, PV membrane; IMS, intermembrane space.

the OMM that can have toxic consequences for the cell (fig. S18) (*4*, *37*). In the context of infection, however, the constant formation of SPOTs mediates the removal of OMM proteins, including SAM50 and TOM20, which are key components of import machinery, and MFN1 and MFN2, which mediate mitochondrial nutrient competition (Fig. 6K) (*5*).

Discussion

Our data showing that stress linked to the import of OMM proteins leads to the shedding of the OMM during and independently of infection opens several questions, including whether differences in the underlying mechanism of OMM remodeling in these scenarios exist. OMM-GFP expression induced the formation of structures in a manner consistent with our description of infection-induced SPOTs. However, the OMM was remodeled in a different manner during *SAM50* silencing/depletion. Whether the smaller *SAM50* silencing/depletion–induced structures are a consequence of defective import of OMM proteins that mediate the emergence of SPOTs or represent other classes of structures that emerge from the OMM, such as MDCs and MDVs, is unclear. Furthermore, what is the nature of the TgMAF1- or OMM-GFP–derived stress that leads to OMM remodeling? Although most known for its role in the biogenesis of β-barrel proteins, SAM50 in yeast can cooperate with the mitochondrial import (MIM) complex that inserts C-tail α-helical proteins into the OMM (*45*). Thus, similar machinery in mammals—so far unknown—may facilitate an interaction between the C-terminal α-helix of TgMAF1 or the OMM-targeting α-helical TM domain of OMM-GFP with SAM50 (*28*). Because SAM50 is the only component of the OMM import machinery with a defined role in bridging the OMM and IMM, perhaps SAM50 can thus function as a sensor that translates stress linked to the import of OMM proteins into a removal of compromised import machinery of the OMM through the disruption of the MIB complex. Additionally, ER whorls that are morphologically similar to SPOTs and contain the ER import translocon have been observed after induction of ER stress (*46*).

What regulates the extent to which the OMM is shed? SNX9 is required for the emergence of a subclass of MDVs that are uniformly shaped and range between 80 and 120 nm in diameter (*22*–*24*). We found that infection induced much

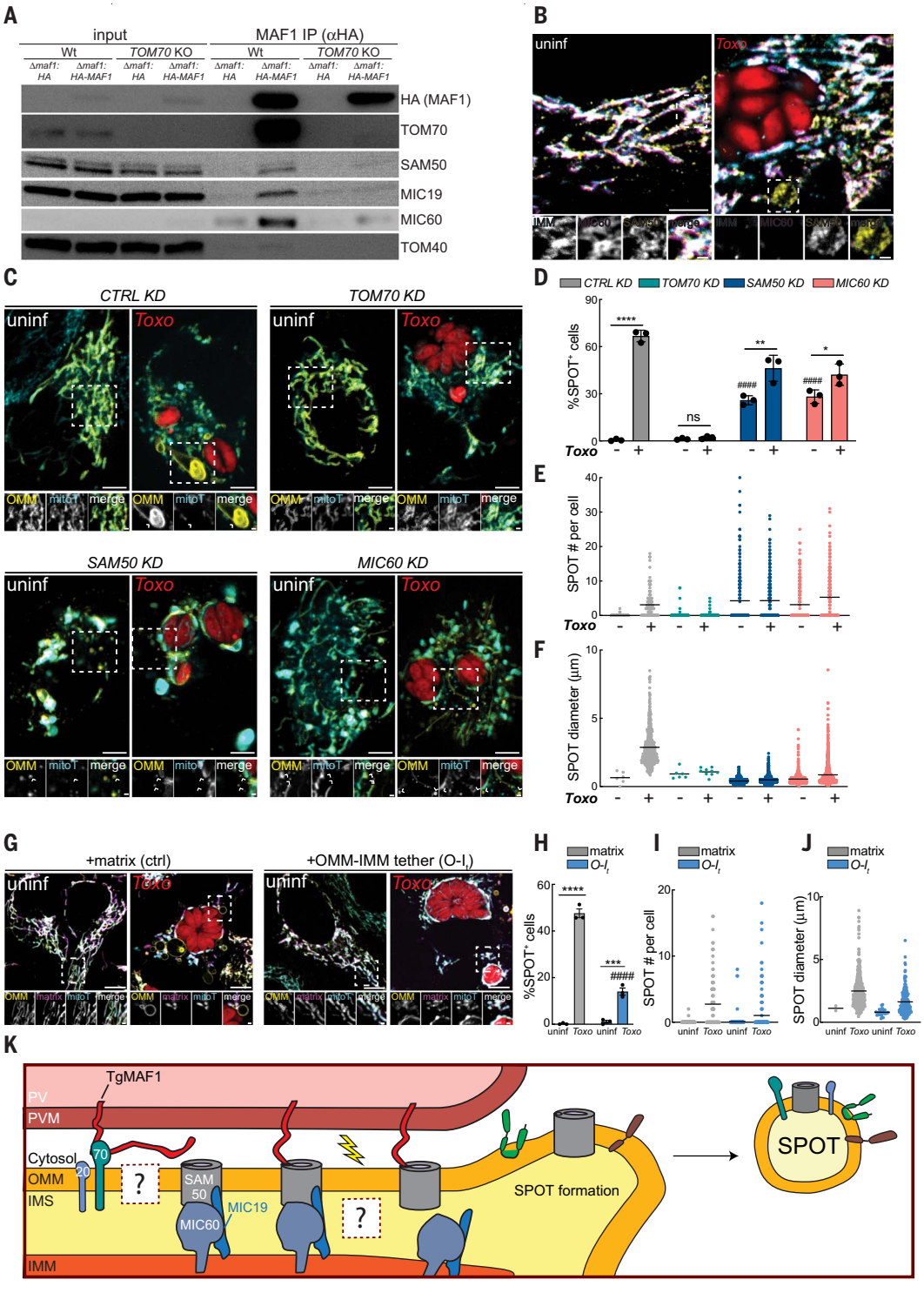

Fig. 6. SAM50 loss of function mediates SPOT formation during infection. (**A**) Anti-HA IPs were prepared from WT and *TOM70 KO* HeLas infected with Δ*maf1*:HA or Δ*maf1*:HA-MAF1 parasites and analyzed for TgMAF1, ~60 kDa; TOM70, ~72 kDa; SAM50, ~55 kDa; MIC60, ~88 kDa; MIC19, ~25 kDa; TOM40, ~40 kDa. (**B**) Representative IF images of uninf and *Toxo* HFFs at 24 hours after infection. (Inset) SPOT in *Toxo*-infected cell contains SAM50 but not MIC60 or ATP51B (IMM). Scale bars, 5 µm and (inset) 1 µm. (**C**) Representative live-cell images of the OMM (BFP) in uninf and *Toxo*-infected *CTRL*, *TOM70*-, *SAM50*-, and *MIC60*-suppressed (KD) HeLas labeled with mitoT. (Insets) SPOTs are indicated with arrowheads. Scale bars, 5 µm and (inset) 1 µm. (**D**) Percentage (%) of SPOT-positive cells in experiments as in (C); data are mean ± SEM of more than 100 cells counted from $n = 3$ replicates; $^{*}P < 0.05$, $^{**}P < 0.01$, $^{****}P < 0.0001$ for uninf versus inf, $\#\#\#\#P < 0.0001$ for *CTRL KD* versus *SAM50 KD*, *MIC60 KD* by means of two-way ANOVA analysis. (**E** and **F**) Scatterplots with mean (E) number and (F) diameter of SPOTs in experiments as in (C) from more than 30 infected cells from three replicates. (**G**) Representative live-cell images of the OMM (GFP) in uninf and *Toxoplasma* (mCh)–infected U2OS cells expressing matrix-BFP (matrix) or BFP fused to an OMM-IMM tether (O-I_1). (**H**) Percent of SPOT-positive cells in experiments as in (G). Data are mean ± SEM of more than 100 cells counted from $n = 3$ biological replicates; $^{***}P < 0.001$, $^{****}P < 0.0001$ for uninf versus inf, $\#\#\#\#P < 0.0001$ for matrix versus O-I_1 by two-way ANOVA analysis. (**I** and **J**) Scatterplots with mean (I) number and (J) diameter of SPOTs in experiments as in (G) from more than 30 infected cells from three replicates. (**K**) Model of SPOT formation: TOM70 (70) mediates the interaction between MAF1 and SAM50 and/or a hypothetical translocase (?), which induces a disassembly of the MIB complex (SAM50, MIC60, and MIC19) and SPOT formation. The constitutive shedding of SPOTs depletes OMM proteins that restrict parasite growth (MFN1 and MFN2) and sequesters import machinery required for mitochondrial biogenesis on SPOTs.

larger SPOTs that range up to 10 µm in diameter, are also SNX9-dependent, and vary in substructure and shape. What factors dictate their morphology and the fate of their proteins? Although MFN1 and MFN2 are targeted for degradation, it remains possible that other SPOT-localized proteins such as SAM50, TOM70, and TOM20 are recycled into the mitochondrial network. SPOTs being oftentimes multivesicular and containing proteins required for fusion (MFNs) and trafficking (MIROs) raises the possibility that these structures might be able to fuse with one another, or with mitochondria to reintegrate into the mitochondrial network.

Whether other pathogen effector proteins coopt host import receptors for their function, analogous to how TgMAF1 exploits host TOM70, is little explored. Pathogens such as *Toxoplasma* might target SAM50 and TOM70, key regulators of mitochondrial import, to impede the biogenesis of organelles that function as nutrient competitors or immune signaling hubs during infection (*5*–*7*). Severe acute respiratory syndrome coronavirus 2 (SARS-CoV-2) encodes for a protein of unknown function (Orf9b) that binds TOM70 to suppress antiviral interferon responses (*47*). Host TOM complex components also mediate contact sites between mitochondria and the vacuole in which *Chlamydia* resides, but whether this bacterium inhibits TOM receptors or induces SPOT formation is not known (*48*).

Our study of the interaction between the human parasite *Toxoplasma* and host mitochondria led to the discovery of a mechanism by which the OMM is remodeled: the formation of SPOTs. These findings shed light on a potentially broader mechanism of organellar response to import-related stress and reveal a strategy by which diverse pathogens may disrupt mitochondrial function.

Materials and methods

Cell culture and cell lines

All cell lines were cultured in complete DMEM (cDMEM: DMEM and 10% heat-inactivated FBS). Cells were tested every 2 weeks for *Mycoplasma* infection by means of polymerase chain reaction (PCR). Details of cell lines generated (including single-guide RNA sequences), used, and origin are in the supplementary materials.

Parasite culture and strains

Toxoplasma gondii parasites were maintained by serial passage in human foreskin fibroblast (HFF) monolayers in cDMEM. Details of parasite lines generated, used, and origin are in the supplementary materials.

Plasmid descriptions, transfections, and siRNA treatment

For transient expression, cells were transfected ~12 hours prior to infection using X-tremeGene reagent (Sigma) per manufacturer's instructions, lipofectamine RNAiMax (Invitrogen) was used per manufacturer's instructions for siRNA treatment. Details of plasmids generated, used, and origin are in the supplementary materials.

Lentiviral production generation of cells stably expressing cDNAs

For production of 293T human embryonic kidney (HEK) cells were transfected using the X-tremeGENE 9 DNA Transfection Reagent (Roche) with 1 μg psPAX2 packaging vector (Addgene #12260), 0.3 μg pCMV-VSVG envelope vector (Addgene #8454) and 1 μg of the relevant plasmid of interest. The next day, the medium was exchanged, and two days post transfection, the virus-containing supernatant was filtered with a 0.45 μM filter and supplemented with polybrene to a final concentration of 5 μg/ml. The virus-containing filtrate was added to 50,000 target cells and exchanged for cDMEM the next day. MEFs, HeLas, U2OS cells were subsequently selected with 8 to 10 μg/ml blasticidin, or 1-2 μg/ml puromycin for 3-5 days. To isolate cells positive for expression of fluorescent protein, transduced cells were sorted for low and high GFP positivity as indicated.

Live cell imaging

Cells were plated on 35mm, 6-well, or 24-well CELLview glass bottom cell culture dishes (Greiner Bio-One), treated as indicated in text (i.e., infection, transfection, 25 mM CCCP treatment for 30 min, or fixation and permeabilization while imaging), and imaged using an Olympus IXplore SpinSR 50 mm spinning disk confocal microscope. Live cell imaging was performed in cDMEM with incubation at 37°C and 5% CO_2. All images were taken with a 100X/1.35 silicon oil objective and excitation with either 405, 488, 561, or 640 laser lines, using ORCA-Flash4.0 cameras (Hamatsu), and cellSens Software. Details of mitotracker and FL-HPC labeling, immunofluorescence analysis, and antibodies used are in the supplementary materials.

Yeast strains, growth conditions, and expression plasmids

The yeast strains used in this study are based on *Saccharomyces cerevisiae* BY4741 (EUROSCARF). Yeast cells were cultured using standard protocols on SC-Leucin (0.67% [w/v] yeast nitrogen base with ammonium sulfate; 0.07% [w/v] amino acid mixture) with 2% [w/v] galactose. Cultures were grown at 30°C until early logarithmic growth phase, which was determined based on the optical density at a wavelength of 600 nm. Full details of strains used and generated, isolation of yeast and mammalian mitochondria, affinity purification of HA-MAF1 from yeast, in vitro binding to TOM70, and in vitro protein import into yeast and mammalian mitochondria in supplementary material.

Line scan analyses

Line-scan analysis of relative fluorescence intensity was performed by measuring pixel intensity across an indicated line using Fiji software.

Immunoprecipitation of mitochondria

Seven million to 8 million MEFs or 293Ts cells were plated in a 15 cm dish and the following day, cells were either mock-infected or infected with *Toxoplasma* (RH$\Delta ku80{:}mCherry^{+}$) at a multiplicity of infection (MOI) of 5. 24 hpi, cells were scraped rinsed 2X in chilled 1X PBS, scraped in 1X chilled PBS supplemented with a protease and inhibitor cocktail (Thermo Scientific a32961) and Phosstop phosphatase inhibitors (Sigma 4906837001)(1XPBS+Inh). Harvested cells were centrifuged at 1000xg for 2 min at 4C and resuspended in 1 ml 1X PBS with inhibitors. 50 μl were collected for the whole cell fraction and the rest was triturated 10X on ice using a 1 ml syringe and $27^{3/4}$ gauge needle. Lysed cells were centrifuged at 1000xg for 2 min at 4C. Cleared lysate was added to 150ul anti-HA bead slurry that had previously been rinsed 3X in 1X PBS and resuspended in 100 μl 1X PBS. Subsequently, mitochondria were immunopurified as previously described and processed for immunoblot analysis or mass spectrometry analysis (*13*). More details on immunoblot analysis and proteomics sample preparation are provided in the supplementary materials.

Flow cytometry analysis

Monolayers of U2OS cells expressing OMM-GFP were rinsed with PBS, trypsinized and fixed in 2% paraformaldehyde in FACS buffer (3% FBS in PBS) for 10 min. After a brief spin, cells were resuspended in FACS buffer and sorted on a FACSAria Fusion Cell Sorter (BD Biosciences) GFP mean fluorescence intensity (mFI) using BD FACSDiva software. ~250,000 cells were sorted into low and high (20× greater than low) GFP bins and transferred to a cell culture dish for continued passaging.

Immunoprecipitation of HA-MAF1 or TOM70

Seven million to 8 million TOM70-expressing MEFs or U2OS cells were infected with *Toxoplasma* at an MOI of 7. 24 hpi cells were rinsed 2X in chilled 1X PBS, scraped down in chilled 1XPBS+Inh, centrifuged at 1000xg for 2 min, and resuspended in lysis buffer for 15 min at 4°C. Cleared lysates were incubated with either 80 μl magnetic anti-HA-beads (Thermo Scientific) or 25 μl magnetic anti-GFP-nanobodies (Chromotek) overnight. The beads were washed 3x times with 1XPBS +Inh. Afterwards, the samples were eluted from the magnetic beads with 2X SDS buffer by incubating them at 40°C for 10 min. Samples were processed for gel electrophoresis and probed with indicated antibodies. For more details on proteomics sample preparation, please see supplementary materials.

Statistical analyses

All statistical analyses were performed using one-way analysis of variance (ANOVA), two-way ANOVA, or an unpaired *t* test in GraphPad Prism 9 software and are indicated accordingly. Volcano plot rendering of proteomics of whole-cell and immunopurified mitochondria fractions are provided in the main and supplementary figures.

REFERENCES AND NOTES

1. L. Pernas, L. Scorrano, Mito-morphosis: Mitochondrial fusion, fission, and cristae remodeling as key mediators of cellular function. *Annu. Rev. Physiol.* **78**, 505–531 (2016). doi: 10.1146/annurev-physiol-021115-105011; pmid: 26667075
2. S. Rath *et al.*, MitoCarta3.0: An updated mitochondrial proteome now with sub-organelle localization and pathway annotations. *Nucleic Acids Res.* **49** (D1), D1541–D1547 (2021). doi: 10.1093/nar/gkaa1011; pmid: 33174596
3. J. A. MacKenzie, R. M. Payne, Mitochondrial protein import and human health and disease. *Biochim. Biophys. Acta* **1772**, 509–523 (2007). doi: 10.1016/j.bbadis.2006.12.002; pmid: 17300922
4. J. Song, J. M. Herrmann, T. Becker, Quality control of the mitochondrial proteome. *Nat. Rev. Mol. Cell Biol.* **22**, 54–70 (2021). doi: 10.1038/s41580-020-00300-2; pmid: 33093673
5. L. Pernas, C. Bean, J. C. Boothroyd, L. Scorrano, Mitochondria restrict growth of the intracellular parasite *Toxoplasma gondii* by limiting its uptake of fatty acids. *Cell Metab.* **27**, 886–897.e4 (2018). doi: 10.1016/j.cmet.2018.02.018; pmid: 29617646
6. V. Tiku, M. W. Tan, I. Dikic, Mitochondrial functions in infection and immunity. *Trends Cell Biol.* **30**, 263–275 (2020). doi: 10.1016/j.tcb.2020.01.006; pmid: 32200805
7. L. Pernas, Cellular metabolism in the defense against microbes. *J. Cell Sci.* **134**, jcs252023 (2021). doi: 10.1242/jcs.252023; pmid: 33558420
8. R. B. Seth, L. Sun, Z. J. Chen, Antiviral innate immunity pathways. *Cell Res.* **16**, 141–147 (2006). doi: 10.1038/sj.cr.7310019; pmid: 16474426
9. T. Rudel, O. Kepp, V. Kozjak-Pavlovic, Interactions between bacterial pathogens and mitochondrial cell death pathways. *Nat. Rev. Microbiol.* **8**, 693–705 (2010). doi: 10.1038/nrmicro2421; pmid: 20818415
10. J. G. Montoya, O. Liesenfeld, Toxoplasmosis. *Lancet* **363**, 1965–1976 (2004). doi: 10.1016/S0140-6736(04)16412-X; pmid: 15194258
11. T. C. Medeiros, C. Mehra, L. Pernas, Contact and competition between mitochondria and microbes. *Curr. Opin. Microbiol.* **63**, 189–194 (2021). doi: 10.1016/j.mib.2021.07.014; pmid: 34411806
12. M. Dumoux, R. D. Hayward, Membrane contact sites between pathogen-containing compartments and host organelles. *Biochim. Biophys. Acta* **1861** (8 Pt B), 895–899 (2016). doi: 10.1016/j.bbalip.2016.01.018; pmid: 26825687
13. W. W. Chen, E. Freinkman, D. M. Sabatini, Rapid immunopurification of mitochondria for metabolite profiling and absolute quantification of matrix metabolites. *Nat. Protoc.* **12**, 2215–2231 (2017). doi: 10.1038/nprot.2017.104; pmid: 29532801
14. V. Soubannier *et al.*, A vesicular transport pathway shuttles cargo from mitochondria to lysosomes. *Curr. Biol.* **22**, 135–141 (2012). doi: 10.1016/j.cub.2011.11.057; pmid: 22226745
15. A. L. Hughes, C. E. Hughes, K. A. Henderson, N. Yazvenko, D. E. Gottschling, Selective sorting and destruction of mitochondrial membrane proteins in aged yeast. *eLife* **5**, e13943 (2016). doi: 10.7554/eLife.13943; pmid: 27097106
16. A. M. English *et al.*, ER-mitochondria contacts promote mitochondrial-derived compartment biogenesis. *J. Cell Biol.* **219**, e202002144 (2020). doi: 10.1083/jcb.202002144; pmid: 33090183
17. M. H. Schuler *et al.*, Mitochondrial-derived compartments facilitate cellular adaptation to amino acid stress. *Mol. Cell* **81**, 3786–3802.e13 (2021). doi: 10.1016/j.molcel.2021.08.021; pmid: 34547239
18. M. Neuspiel *et al.*, Cargo-selected transport from the mitochondria to peroxisomes is mediated by vesicular carriers. *Curr. Biol.* **18**, 102–108 (2008). doi: 10.1016/j.cub.2007.12.038; pmid: 18207745
19. M. H. Schuler, A. M. English, L. VanderMeer, J. M. Shaw, A. L. Hughes, Amino acids promote mitochondrial-derived compartment formation in mammalian cells. bioRxiv [Preprint] 23 December 2020. .doi: 10.1101/2020.12.23.424218
20. G. L. McLelland, V. Soubannier, C. X. Chen, H. M. McBride, E. A. Fon, Parkin and PINK1 function in a vesicular trafficking pathway regulating mitochondrial quality control. *EMBO J.* **33**, 282–295 (2014). doi: 10.1002/embj.201385902; pmid: 24446486
21. S. R. Denison *et al.*, Alterations in the common fragile site gene Parkin in ovarian and other cancers. *Oncogene* **22**, 8370–8378 (2003). doi: 10.1038/sj.onc.1207072; pmid: 14614460
22. D. Matheoud *et al.*, Parkinson's disease-related proteins PINK1 and parkin repress mitochondrial antigen presentation. *Cell* **166**, 314–327 (2016). doi: 10.1016/j.cell.2016.05.039; pmid: 27345367
23. R. Lundmark, S. R. Carlsson, SNX9—A prelude to vesicle release. *J. Cell Sci.* **122**, 5–11 (2009). doi: 10.1242/jcs.037135; pmid: 19092055
24. K. Todkar *et al.*, Selective packaging of mitochondrial proteins into extracellular vesicles prevents the release of mitochondrial DAMPs. *Nat. Commun.* **12**, 1971 (2021). doi: 10.1038/s41467-021-21984-w; pmid: 33785738
25. A. P. Sinai, P. Webster, K. A. Joiner, Association of host cell endoplasmic reticulum and mitochondria with the *Toxoplasma gondii* parasitophorous vacuole membrane: A high affinity interaction. *J. Cell Sci.* **110**, 2117–2128 (1997). doi: 10.1242/jcs.110.17.2117; pmid: 9378762
26. L. Scorrano *et al.*, Coming together to define membrane contact sites. *Nat. Commun.* **10**, 1287 (2019). doi: 10.1038/s41467-019-09253-3; pmid: 30894536
27. L. Pernas *et al.*, Toxoplasma effector MAF1 mediates recruitment of host mitochondria and impacts the host response. *PLOS Biol.* **12**, e1001845 (2014). doi: 10.1371/journal.pbio.1001845; pmid: 24781109
28. M. L. Blank *et al.*, A *Toxoplasma gondii* locus required for the direct manipulation of host mitochondria has maintained multiple ancestral functions. *Mol. Microbiol.* **108**, 519–535 (2018). doi: 10.1111/mmi.13947; pmid: 29505111
29. F. D. Kelly *et al.*, *Toxoplasma gondii* MAF1b binds the host cell MIB complex to mediate mitochondrial association. *MSphere* **2**, e00183-17 (2017). doi: 10.1128/mSphere.00183-17; pmid: 28567444
30. M. Suzuki, O. Danilchanka, J. J. Mekalanos, Vibrio cholerae T3SS effector VopE modulates mitochondrial dynamics and innate immune signaling by targeting Miro GTPases. *Cell Host Microbe* **16**, 581–591 (2014). doi: 10.1016/j.chom.2014.09.015; pmid: 25450857
31. B. Mueller, E. J. Klemm, E. Spooner, J. H. Claessen, H. L. Ploegh, SEL1L nucleates a protein complex required for dislocation of misfolded glycoproteins. *Proc. Natl. Acad. Sci. U.S.A.* **105**, 12325–12330 (2008). doi: 10.1073/pnas.0805371105; pmid: 18711132
32. N. C. Chan *et al.*, Broad activation of the ubiquitin-proteasome system by Parkin is critical for mitophagy. *Hum. Mol. Genet.* **20**, 1726–1737 (2011). doi: 10.1093/hmg/ddr048; pmid: 21296869
33. S. Nahar, A. Chowdhury, T. Ogura, M. Esaki, A AAA ATPase Cdc48 with a cofactor Ubx2 facilitates ubiquitylation of a mitochondrial fusion-promoting factor Fzo1 for proteasomal degradation. *J. Biochem.* **167**, 279–286 (2020). doi: 10.1093/jb/mvz104; pmid: 31804690
34. M. K. Shaw, C. Y. He, D. S. Roos, L. G. Tilney, Proteasome inhibitors block intracellular growth and replication of *Toxoplasma gondii*. *Parasitology* **121**, 35–47 (2000). doi: 10.1017/S0031182099006071; pmid: 11085223
35. M. L. Blank *et al.*, *Toxoplasma gondii* association with host mitochondria requires key mitochondrial protein import machinery. *Proc. Natl. Acad. Sci. U.S.A.* **118**, e2013336118 (2021). doi: 10.1073/pnas.2013336118; pmid: 33723040
36. S. Backes *et al.*, Tom70 enhances mitochondrial preprotein import efficiency by binding to internal targeting sequences. *J. Cell Biol.* **217**, 1369–1382 (2018). doi: 10.1083/jcb.201708044; pmid: 29382700
37. S. Backes *et al.*, The chaperone-binding activity of the mitochondrial surface receptor Tom70 protects the cytosol against mitoprotein-induced stress. *Cell Rep.* **35**, 108936 (2021). doi: 10.1016/j.celrep.2021.108936; pmid: 33826901
38. A. C. Fan, M. K. Bhangoo, J. C. Young, Hsp90 functions in the targeting and outer membrane translocation steps of Tom70-mediated mitochondrial import. *J. Biol. Chem.* **281**, 33313–33324 (2006). doi: 10.1074/jbc.M605250200; pmid: 16968702
39. H. Yamamoto *et al.*, Roles of Tom70 in import of presequence-containing mitochondrial proteins. *J. Biol. Chem.* **284**, 31635–31646 (2009). doi: 10.1074/jbc.M109.041756; pmid: 19767391
40. C. Ott *et al.*, Sam50 functions in mitochondrial intermembrane space bridging and biogenesis of respiratory complexes. *Mol. Cell. Biol.* **32**, 1173–1188 (2012). doi: 10.1128/MCB.06388-11; pmid: 22252321
41. M. P. Viana, R. M. Levytskyy, R. Anand, A. S. Reichert, O. Khalimonchuk, Protease OMA1 modulates mitochondrial bioenergetics and ultrastructure through dynamic association with MICOS complex. *iScience* **24**, 102119 (2021). doi: 10.1016/j.isci.2021.102119; pmid: 33644718
42. D. V. Dabir *et al.*, A small molecule inhibitor of redox-regulated protein translocation into mitochondria. *Dev. Cell* **25**, 81–92 (2013). doi: 10.1016/j.devcel.2013.03.006; pmid: 23597483
43. U. Bömer *et al.*, The sorting route of cytochrome b2 branches from the general mitochondrial import pathway at the preprotein translocase of the inner membrane. *J. Biol. Chem.* **272**, 30439–30446 (1997). doi: 10.1074/jbc.272.48.30439; pmid: 9374535
44. M. Eilers, G. Schatz, Binding of a specific ligand inhibits import of a purified precursor protein into mitochondria. *Nature* **322**, 228–232 (1986). doi: 10.1038/322228a0; pmid: 3016548
45. K. N. Doan *et al.*, The mitochondrial import complex MIM functions as main translocase for α-helical outer membrane proteins. *Cell Rep.* **31**, 107567 (2020). doi: 10.1016/j.celrep.2020.107567; pmid: 32348752
46. F. Xu *et al.*, COPII mitigates ER stress by promoting formation of ER whorls. *Cell Res.* **31**, 141–156 (2021). doi: 10.1038/s41422-020-00416-2; pmid: 32989223
47. C. U. Mårtensson *et al.*, Mitochondrial protein translocation-associated degradation. *Nature* **569**, 679–683 (2019). doi: 10.1038/s41586-019-1227-y; pmid: 31118508
48. I. Derré, M. Pypaert, A. Dautry-Varsat, H. Agaisse, RNAi screen in Drosophila cells reveals the involvement of the Tom complex in Chlamydia infection. *PLOS Pathog.* **3**, 1446–1458 (2007). doi: 10.1371/journal.ppat.0030155; pmid: 17967059

ACKNOWLEDGMENTS

We thank N. Laqtom and M. A. Remaileh (Stanford University) for teaching us the mitoIP protocol; T. Langer (MPI-AGE) for the generous sharing of reagents; the MPI-AGE Proteomics Core, in particular X. Li for advice on sample preparation; the MPI-AGE FACS and Imaging Core for excellent flow cytometry, and microscopy support, and in particular M. Kirchner; and the CECAD imaging facility and in particular K. Seidel for electron microscopy support. We also thank S. Reato for excellent laboratory support, P. Krueger for manuscript feedback, and all members of the Pernas laboratory for helpful discussions. **Funding:** This work was supported by the European Research Council ERC-StG-2019 852457 (to L.F.P.); Deutsche Forschungsgemeinschaft SFB 1218 Project ID 269925409 (to L.F.P. and T.B.); Project ID 411422114–GRK 2550 (to L.F.P.); BE 4679/2-2 Project ID 269424439 (to T.B.); BONFOR program of the Univeristy Hospital Bonn (to F.d.B.); Chinese Research Council (to X.L.); and IMPRS (to C.M.). **Author contributions:** Conceptualization: X.L., J.S., and L.F.P. Methodology: X.L., J.S., T.C.M., C.M., F.d.B., E.P., K.S., J.R., T.B., and L.F.P. Investigation: All authors. Resources: E.B., C.A., J.B.M., and C.M. Proteomics analysis: X.L., L.F.P., and I.A. Funding acquisition: X.L. and L.F.P. Project administration: L.F.P. Writing, original draft: X.L. and L.F.P. Writing, review and editing: All authors. Supervision: L.F.P. **Competing interests:** The authors declare that they have no competing interests. **Data and materials availability:** OMM-GFP–expressing *Miro1*$^{+/+}$*2*$^{+/+}$ *Miro1*$^{-/-}$*2*$^{-/-}$ MEFs; Ctrl; OMM-BFP–expressing SAM50-, MIC60-, and TOM70-suppressed HeLas; and the OMM-IMM tether were acquired under a materials transfer agreement with University College London, University of Wuerzburg, and University of Nebraska–Lincoln, respectively. The mass spectrometry proteomics data have been deposited to the ProteomeXchange Consortium through the PRIDE partner repository with the dataset identifier PXD024491.

SUPPLEMENTARY MATERIALS

science.org/doi/10.1126/science.abi4343
Materials and Methods
Figs. S1 to S18
References (*49*–*62*)
Data Files S1 to S3
Movies S1 and S2

View/request a protocol for this paper from *Bio-protocol*.

11 March 2021; resubmitted 4 October 2021
Accepted 22 November 2021
10.1126/science.abi4343